Multifrequency Microwave Tomography in Lebesgue Spaces With Nonconstant Exponents

Alessandro Fedeli, Claudio Estatico, Andrea Randazzo, and Matteo Pastorino

Abstract — This article proposes an inversion method for microwave tomography that combines a multifrequency data processing with a nonlinear regularization procedure formulated in Lebesgue spaces with nonconstant exponents. In order to fully take advantage of frequency diversity, scattered-field data measured at different frequencies are jointly processed inside the inversion algorithm. The performance of the proposed method versus the range of the Lebesgue-space exponent function is assessed from an experimental viewpoint by considering both homogeneous and inhomogeneous targets from the well-known Fresnel data sets.

1. Introduction

Although quantitative microwave tomography has emerged as a promising diagnostic tool in several fields, the underlying inverse scattering problem is still considered very challenging to solve, especially when its nonlinear nature is taken into account [1]. In this context, it is desirable to exploit all the available information in an effective and computationally efficient way. One of the key points that may aid the resolution of such an inverse problem is making use of frequency diversity [2]. Undeniably, several applications may benefit from the processing of multifrequency data, from biomedical imaging to civil engineering [3–6].

In this framework, multifrequency inversion techniques have also been shown to provide good results when combined with regularization strategies outside the conventional setting of Hilbert spaces [7]. At present, however, such techniques still suffer from the limitation of using constant values for the L^p space exponent p, which are highly dependent on the configuration and not easy to predict without knowledge of the actual target. A step forward toward the solution of this problem has been done with the introduction of a microwave imaging approach in Lebesgue space with nonconstant exponents [8]. In this technique, the exponent parameter is pointwise defined inside the investigation domain by the inversion method itself in an adaptive way based on reconstruction results at each inexact-Newton iteration. So far, this approach has been used only in single-frequency [8] or frequency-hopping schemes [9]. In this article, an extension of this technique for simultaneously processing multifrequency data is proposed for the first time. The developed approach is experimentally validated by using the Fresnel data sets in five different test cases, including both homogeneous and inhomogeneous target configurations. The effect of changing the range of the exponent variation has also been analyzed considering different ranges of operating frequencies.

Manuscript received 26 August 2020.

Alessandro Fedeli, Matteo Pastorino, and Andrea Randazzo are with the Department of Electrical, Electronic, Telecommunications Engineering, and Naval Architecture, University of Genoa, via all'Opera Pia 11A, 16145 Genoa, Italy; e-mail: alessandro.fedeli@unige.it, matteo.pastorino@unige.it, andrea.randazzo@unige.it.

Claudio Estatico is with the Department of Mathematics, University of Genoa, via Dodecaneso 35, 16146 Genoa, Italy; e-mail: estatico@dima.unige.it.

2. Formulation of the Multifrequency Inversion Method

A tomographic configuration is considered in this article under the hypotheses of transverse-magnetic illumination at F different frequencies ($f_1, \ldots, f_F$) and homogeneous dielectric properties of the object under test (OUT) along the axial coordinate. The horizontal cross section of the OUT is contained inside the investigation domain $\mathbb{D}_{\text{inv}}$. The goal of the inverse problem solution is to find the dielectric properties of the OUT, which are described by an unknown function $x = [(\epsilon_r(\mathbf{r}) - 1) \quad \sigma(\mathbf{r})/(2\pi f_1 \epsilon_0)]^T$ for $\mathbf{r} \in \mathbb{D}_{\text{inv}}$, where $\epsilon_r(\mathbf{r})$, $\sigma(\mathbf{r})$, and ϵ_0 are the relative dielectric permittivity of the OUT, its electric conductivity, and the dielectric permittivity of vacuum, respectively.

Scattered-field data at each frequency Δu_f ($f = f_1, \ldots, f_F$) are sampled by a proper set of electric field probes in an external observation domain $\mathbb{O}$ lying on the same plane as the illuminating antennas. When the above assumptions hold, a scalar and two-dimensional electromagnetic problem can be stated, for each probing frequency f, as

$$\mathcal{F}_f\left(W_f x\right) - \Delta u_f = 0 \tag{1}$$

where the nonlinear operator $\mathcal{F}_f$ derives from the scattering phenomena [1] and $W_f = [\,1 - jf_1/f\,]$. In order to jointly exploit the available multifrequency data, a system of equations is formulated as

$$\underbrace{\begin{bmatrix} \Re\left\{\mathcal{F}_{f_1}\left(W_{f_1}x\right)\right\} \\ \Im\left\{\mathcal{F}_{f_1}\left(W_{f_1}x\right)\right\} \\ \vdots \\ \Re\left\{\mathcal{F}_{f_F}\left(W_{f_F}x\right)\right\} \\ \Im\left\{\mathcal{F}_{f_F}\left(W_{f_F}x\right)\right\} \end{bmatrix}}_{\mathcal{F}_{\text{MF}}(x)} - \underbrace{\begin{bmatrix} \Re\left\{\Delta u_{f_1}\right\} \\ \Im\left\{\Delta u_{f_1}\right\} \\ \vdots \\ \Re\left\{\Delta u_{f_F}\right\} \\ \Im\left\{\Delta u_{f_F}\right\} \end{bmatrix}}_{\Delta u_{\text{MF}}} = 0 \tag{2}$$

It is worth noting that since the unknown $x \in X$ is real-valued, the resulting problem is formed by

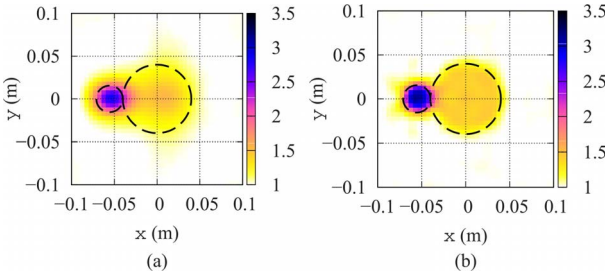

Figure 1. Reconstructed distributions of the relative dielectric permittivity of the FoamDielExtTM target obtained with (a) single-frequency processing ($F = 1$, $f = 2$ GHz, $\Delta p = 0.6$) and (b) multi-frequency processing ($F = 9, f = \{2, \ldots, 10\}$GHz, $\Delta p = 0.4$).

separating real and imaginary parts $\Re$ and $\Im$. Equation (2) also defines the set of multifrequency scattered field data $\Delta u_{\mathrm{MF}} \in Y$ and a scattering operator $\mathcal{F}_{\mathrm{MF}} : X \to Y$.

A full-wave inversion approach in Lebesgue spaces $L^{p(\cdot)}$ with nonconstant exponent $p(\cdot)$ (described in [8] for the single-frequency case) is proposed here to solve such a nonlinear problem. In the present case, the space of unknown X is a nonconstant-exponent Lebesgue space $L^{p(\mathbf{r})}$, $\mathbf{r} \in \mathbb{D}_{\mathrm{inv}}$, whereas Y (data space) is a space L^{p_m} with constant exponent p_m, equal to the average value of $p(\mathbf{r})$ inside $\mathbb{D}_{\mathrm{inv}}$.

The inversion algorithm follows an inexact-Newton scheme based on the iterative linearization of (2) around the current estimate of the unknown x. In particular, at the nth Newton step, the linearized equation becomes

$$\mathcal{F}'_{\mathrm{MF},n}\delta_n + \mathcal{F}_{\mathrm{MF}}(x_n) - \Delta u_{\mathrm{MF}} = 0 \qquad (3)$$

where $\mathcal{F}'_{\mathrm{MF},n}$ is the Fréchet derivative of $\mathcal{F}_{\mathrm{MF}}$ at x_n. The unknown of the linear problem (δ_n) is found by the truncated Landweber-type method in $L^{p(\cdot)}$ spaces introduced in [8]. Subsequently, the solution is updated with $x_{n+1} = x_n + \delta_n$. In each Newton iteration, the exponents of Lebesgue spaces X and Y are also adaptively updated. Regarding the space of unknown X, its exponent $p_n(\mathbf{r}), \mathbf{r} \in \mathbb{D}_{\mathrm{inv}}$, is chosen on the basis of the normalized magnitude of the reconstructed unknown function, that is,

$$p_n(\mathbf{r}) = 2 + \Delta p\left[x_n^{\mathrm{NOR}}(\mathbf{r}) - 1\right], \quad \mathbf{r} \in \mathbb{D}_{\mathrm{inv}} \qquad (4)$$

where the constant value $\Delta p \in [0, 1)$ is the range of variation of the function p_n, with normalized unknown at the nth iteration $x_n^{\mathrm{NOR}}(\mathbf{r}) = \|x_n(\mathbf{r})\| / \max_{\mathbf{r}\in\mathbb{D}_{\mathrm{inv}}} \|x_n(\mathbf{r})\|$. According to this equation, p_n assumes values between $2 - \Delta p$ (where $x_n^{\mathrm{NOR}} = 0$, i.e., in points not occupied by the OUT) and 2 (where $x_n^{\mathrm{NOR}} = 1$). In this way, lower values of the exponent function p are assigned outside the OUT and higher values inside. It is important to notice that in the absence of a priori information about the OUT, an empty initial guess $x_0 = 0$ is considered, and the inversion method starts with a constant exponent function $p_0(\mathbf{r}) = 2 - \Delta p$ in its first iteration.

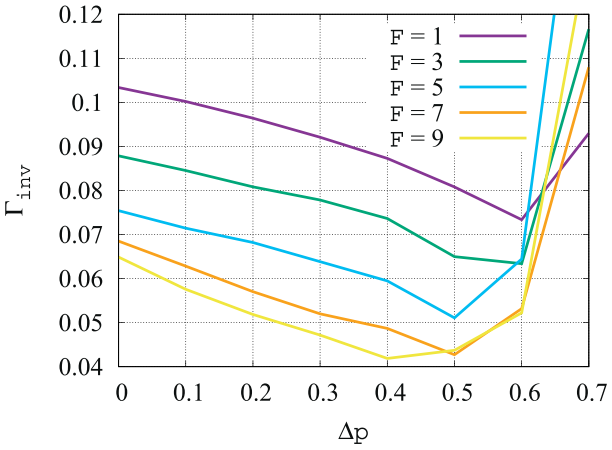

Figure 2. FoamDielExtTM target. Relative reconstruction error on the dielectric permittivity of the whole investigation domain (Γ_{inv}) versus the number of frequencies F and the range of the Lebesgue-space exponent function Δp.

3. Experimental Assessment

The proposed method has been tested against two different experimental data sets of the Institut Fresnel (Marseille, France) [10, 11]. In particular, the three targets FoamDielExtTM, FoamDielIntTM, and FoamTwinDielTM, which constitute inhomogeneous dielectric configurations with quite complex cross sections, were first considered [10]. In all cases, the inversion algorithm has been executed with maximum numbers of Newton and Landweber iterations $N = 50$ and $L = 10$, respectively, and a threshold on the relative variation of the data residual $r_{\mathrm{thr}} = 0.05$. $\mathbb{D}_{\mathrm{inv}}$ is a region of size 0.1 m $\times$ 0.1 m , subdivided into a 40 $\times$ 40 grid of square cells. The incident field inside $\mathbb{D}_{\mathrm{inv}}$ has been modeled using line-current sources directed along the axial coordinate and whose amplitudes have been calibrated by fitting the data available in the measure-

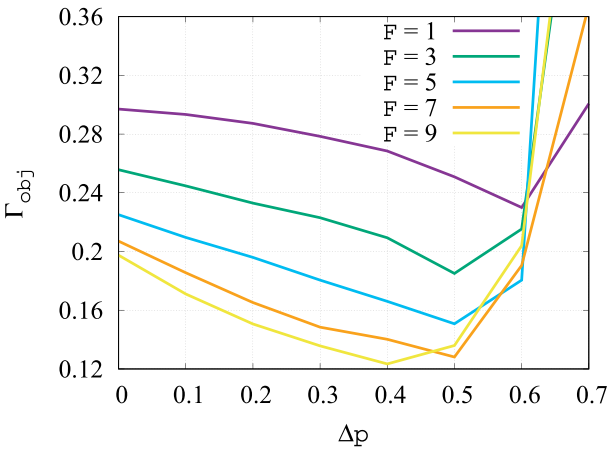

Figure 3. FoamDielExtTM target. Relative reconstruction error on the dielectric permittivity of the target (Γ_{obj}) versus the number of frequencies F and the range of the Lebesgue-space exponent function Δp.

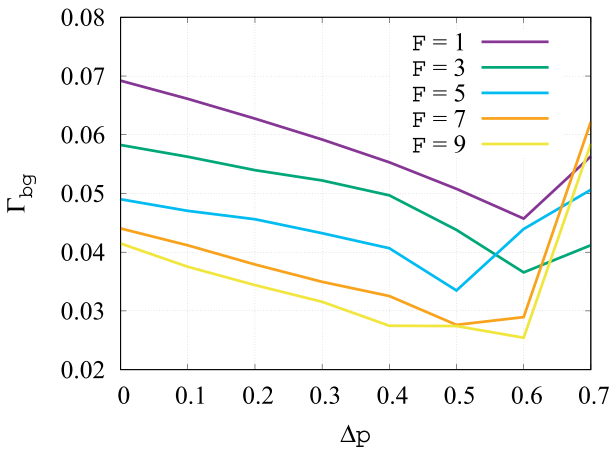

Figure 4. FoamDielExtTM target. Relative reconstruction error on the dielectric permittivity of the background (Γ_{bg}) versus the number of frequencies F and the range of the Lebesgue-space exponent function Δp.

ment points. In the data set [10], the objects are approximately centered at $y = 0$, and frequencies between 2 GHz and 10 GHz have been considered, with 1 GHz step. The scattered electric field is collected in $M = 241$ test points on a 240° arc of circumference with radius $r = 1.67$ m. In the first two cases, $S = 8$ source locations equally spaced on the same circumference are used to illuminate $\mathbb{D}_{inv}$. The FoamDielExtTM target is composed of a foam cylinder (centered at $x_1 = 0$ m, diameter $d_1 = 0.08$ m, relative permittivity $\epsilon_{r,1} = 1.45$) and a plastic cylinder (centered at $x_2 = -0.0555$ m, diameter $d_2 = 0.031$ m, relative permittivity $\epsilon_{r,2} = 3$). The reconstructed distributions of the relative dielectric permittivity retrieved by the single-frequency approach [8] at 2 GHz and by the proposed multifrequency method ($F = 9$ frequencies, $f = \{2, 3, \ldots, 10\}$GHz) are shown in Figure 1a–b. Clearly, a significant advantage is obtained by means of the multifrequency processing, where all the available frequencies are exploited.

The following error metrics have been adopted for comparing results in a quantitative way:

Table 1. FoamDielExtTM target. Relative reconstruction errors (Γ_{inv}, Γ_{obj}, Γ_{bg}), optimal values of the exponent function range (Δp_{opt}), number of performed outer (Newton) iterations, and elapsed time versus the number of frequencies considered inside the inversion procedure

Number of frequencies	Γ_{inv}	Γ_{obj}	Γ_{bg}	Δp_{opt}	Outer iterations	Time[a] (s)
$F = 1$	0.073	0.230	0.046	0.6	6	5.96
$F = 3$	0.063	0.215	0.037	0.6	5	21.07
$F = 5$	0.051	0.151	0.033	0.5	10	45.27
$F = 7$	0.043	0.128	0.028	0.5	6	65.60
$F = 9$	0.042	0.123	0.027	0.4	6	89.75

[a] Elapsed time for each outer iteration on a workstation equipped with a quad-core Intel Core i7-2600K CPU at 3.50 GHz and 8 GB of random-access memory.

Table 2. FoamDielIntTM and FoamTwinDielTM targets. Relative reconstruction errors (Γ_{inv}, Γ_{obj}, Γ_{bg}), optimal values of the exponent function range (Δp_{opt}), and number of performed outer (Newton) iterations versus the number of frequencies considered inside the inversion procedure

Target	Number of frequencies	Γ_{inv}	Γ_{obj}	Γ_{bg}	Δp_{opt}	Outer iterations
FoamDielIntTM	$F = 1$	0.059	0.303	0.022	0.5	5
	$F = 3$	0.053	0.275	0.020	0.5	5
	$F = 5$	0.044	0.226	0.017	0.5	5
	$F = 7$	0.038	0.202	0.013	0.4	6
	$F = 9$	0.033	0.172	0.012	0.4	7
FoamTwinDielTM	$F = 1$	0.102	0.391	0.051	0.5	6
	$F = 3$	0.079	0.299	0.040	0.5	7
	$F = 5$	0.070	0.257	0.037	0.4	7
	$F = 7$	0.059	0.219	0.030	0.4	7
	$F = 9$	0.053	0.198	0.027	0.4	8

$$\Gamma_R = \frac{1}{N_R} \sum_{\mathbf{r}_i \in \mathbb{D}_R} \frac{\left|\epsilon_r(\mathbf{r}_i) - \epsilon_r^a(\mathbf{r}_i)\right|}{\left|\epsilon_r^a(\mathbf{r}_i)\right|} \tag{5}$$

where $R = \{\text{inv, obj, bg}\}$ indicates the considered region, namely, the whole investigation domain ($\mathbb{D}_{inv}$), the region inside the OUT ($\mathbb{D}_{obj}$), and the background ($\mathbb{D}_{bg}$); N_R is the corresponding number of cells; $\epsilon_r(\mathbf{r}_i)$ and $\epsilon_r^a(\mathbf{r}_i)$ are the reconstructed and the actual relative permittivity in the ith cell, respectively.

In order to assess the method performance versus a change in the exponent range Δp, this parameter is varied between 0 (i.e., Hilbert-space reconstruction, constant exponent) and 0.7. The behavior of Γ_{inv}, Γ_{obj}, and Γ_{bg} versus F (number of considered frequencies) and Δp is shown in Figures 2–4.

All error metrics initially reveal a decreasing trend versus Δp, bottom out between 0.6 and 0.4, and then start to rise. The optimal values of Δp based on Γ_{inv} are reported in Table 1 along with reconstruction errors. As expected, errors decrease by including more frequencies. The optimal range Δp_{opt} slightly reduces when F increases but does not exhibit large variations around its average value.

A second test has been performed with the FoamDielIntTM target, which is similar to the previous one except for the position of the second cylinder, in this case centered at $x_2 = -0.005$ m (i.e., plastic cylinder inside the foam one). The error metrics, as

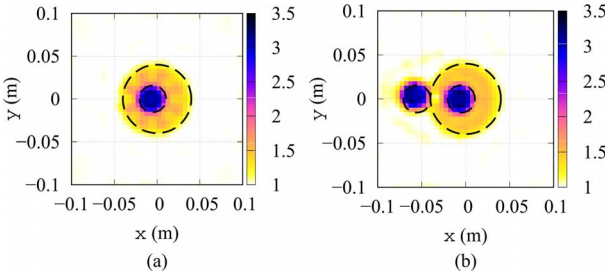

Figure 5. Reconstructed distributions of the relative dielectric permittivity of (a) the FoamDielIntTM target and (b) the FoamTwinDielTM target obtained with multifrequency processing ($F = 9$, $f = \{2, \ldots, 10\}$GHz, $\Delta p = 0.4$).

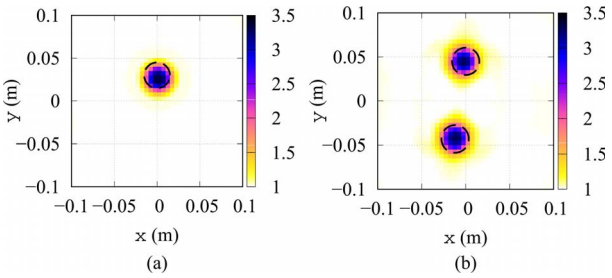

Figure 6. Reconstructed distributions of the relative dielectric permittivity of (a) the DielTM target and (b) the TwoDielTM target obtained with multifrequency processing ($F = 7, f = \{2, \ldots, 8\}$GHz, $\Delta p = 0.5$).

well as the optimal range parameters Δp_{opt}, are reported in Table 2. Results are analogous to the previous situation, and the multifrequency reconstruction of ϵ_r obtained with $F = 9$ frequencies is shown in Figure 5a.

In the third considered case (FoamTwinDielTM target), the measurement configuration is slightly different and has $S = 18$ equally spaced sources. The target is a combination of the former cases and has two identical plastic cylinders at $x_2 = -0.0555$ m and $x_3 = -0.005$ m. The reconstructed dielectric permittivity is presented in Figure 5b, and errors are listed in Table 2. Even in this more challenging case, results confirm the previous observations, and a good reconstruction of the target is achieved.

Finally, we considered the inversion of the targets DielTM and TwoDielTM from the data set [11] by using the mean value of the optimal exponent range (i.e., $\Delta p = 0.5$) based on the previous analysis. The measurement setup is composed of $M = 49$ points on a circumference with radius $r_{\text{RX}} = 0.76$ m, with $S = 36$ equally spaced source locations on a circumference with radius $r_{\text{TX}} = 0.72$ m. $F = 7$ frequencies between 2 GHz and 8 GHz have been considered in this case. Results are reported in Figure 6. As to the DielTM case (plastic cylinder with $\epsilon_r = 3$ and diameter $d_3 = 0.03$ m), the selected range Δp coincides with the optimal one and provides a reconstruction error $\Gamma_{\text{inv}} = 0.027$. With the TwoDielTM target (two cylinders identical to the previous one spaced by 0.09 m), the optimal value of Δp is equal to 0.6 ($\Gamma_{\text{inv}} = 0.052$). However, adopting $\Delta p = 0.5$ yields a result very close to the optimal one, with $\Gamma_{\text{inv}} = 0.058$. This analysis therefore indicates that choosing a mean exponent range based on the initial assessment ensures good results even in the presence of different target configurations and measurement setups.

4. Conclusions

The multifrequency inversion of scattered-field measurements in tomographic configurations has been addressed in this article. An inverse-scattering procedure developed in Lebesgue spaces with nonconstant exponents is extended for the first time to simultaneously process multifrequency data. The proposed approach has been validated by considering five test cases from the Fresnel experimental database, evaluating the effects of the exponent range and the number of included frequencies. The obtained results encourage the use of this technique in various microwave imaging applications (e.g., brain stroke detection, subsurface imaging) as well as its extension to three-dimensional configurations.

5. References

1. M. Pastorino and A. Randazzo, *Microwave Imaging Methods and Applications*, Boston, Artech House, 2018.
2. O. M. Bucci, L. Crocco, T. Isernia, and V. Pascazio, "Inverse Scattering Problems With Multifrequency Data: Reconstruction Capabilities and Solution Strategies," *IEEE Transactions on Geoscience and Remote Sensing*, **38**, 4, July 2000, pp. 1749-1756.
3. W. Zhang, L. Li, and F. Li, "Multifrequency Imaging From Intensity-Only Data Using the Phaseless Data Distorted Rytov Iterative Method," *IEEE Transactions on Antennas and Propagation*, **57**, 1, January 2009, pp. 290-295.
4. M. Salucci, L. Poli, N. Anselmi, and A. Massa, "Multifrequency Particle Swarm Optimization for Enhanced Multiresolution GPR Microwave Imaging," *IEEE Transactions on Geoscience and Remote Sensing*, **55**, 3, March 2017, pp. 1305-1317.
5. S. Sun, B.-J. Kooij, and A. G. Yarovoy, "Inversion of Multifrequency Data With the Cross-Correlated Contrast Source Inversion Method," *Radio Science*, **53**, 6, June 2018, pp. 710-723.
6. C. Kaye, I. Jeffrey, and J. LoVetri, "Improvement of Multi-Frequency Microwave Breast Imaging Through Frequency Cycling and Tissue-Dependent Mapping," *IEEE Transactions on Antennas and Propagation*, **67**, 11, November 2019, pp. 7087-7096.
7. C. Estatico, A. Fedeli, M. Pastorino, and A. Randazzo, "A Multifrequency Inexact-Newton Method in Lp Banach Spaces for Buried Objects Detection," *IEEE Transactions on Antennas and Propagation*, **63**, 9, September 2015, pp. 4198-4204.
8. C. Estatico, A. Fedeli, M. Pastorino, and A. Randazzo, "Quantitative Microwave Imaging Method in Lebesgue Spaces With Nonconstant Exponents," *IEEE Transactions on Antennas and Propagation*, **66**, 12, December 2018, pp. 7282-7294.
9. I. Bisio, C. Estatico, A. Fedeli, F. Lavagetto, M. Pastorino, et al., "Variable-Exponent Lebesgue-Space Inversion for Brain Stroke Microwave Imaging," *IEEE Transactions on Microwave Theory and Techniques*, **68**, 5, May 2020, pp. 1882-1895.
10. J.-M. Geffrin, P. Sabouroux, and C. Eyraud, "Free Space Experimental Scattering Database Continuation: Experimental Set-Up and Measurement Precision," *Inverse Problems*, **21**, 6, December 2005, pp. S117-S130.
11. K. Belkebir and M. Saillard, "Special Section: Testing Inversion Algorithms Against Experimental Data," *Inverse Problems*, **17**, 6, November 2001, pp. 1565-1571.